THE JOURNAL OF BIOLOGICAL CHEMISTRY VOL. 291, NO. 3, pp. 1320–1335, January 15, 2016

Annexin A6 and Late Endosomal Cholesterol Modulate Integrin Recycling and Cell Migration*

Received for publication, August 6, 2015, and in revised form, November 3, 2015 Published, JBC Papers in Press, November 17, 2015, DOI 10.1074/jbc.M115.683557

Ana García-Melero[‡1], Meritxell Reverter[‡1], Monira Hoque[§1], Elsa Meneses-Salas[‡1], Meryem Koese[§2], James R. W. Conway[¶], Camilla H. Johnsen[‡], Anna Alvarez-Guaita[‡], Frederic Morales-Paytuvi[‡], Yasmin A. Elmaghrabi[§], Albert Pol[‖], Francesc Tebar[‡**], Rachael Z. Murray[‡‡], Paul Timpson[¶], Carlos Enrich[‡**3], Thomas Grewal[§4], and Carles Rentero[‡**5]**

*From the [‡]Departament de Biologia Cel·lular, Immunologia i Neurociències, Facultat de Medicina, Universitat de Barcelona, 08036 Barcelona, Spain, [§]Faculty of Pharmacy, University of Sydney, Sydney, New South Wales 2006, Australia, [¶]Garvan Institute of Medical Research and Kinghorn Cancer Centre, Cancer Research Program, St. Vincent's Clinical School, Faculty of Medicine, University of New South Wales, Sydney, New South Wales 2010, Australia, [‖]Institució Catalana de Recerca i Estudis Avançats (ICREA), 08010 Barcelona, Spain, **Centre de Recerca Biomèdica CELLEX, Institut d'Investigacions Biomèdiques August Pi i Sunyer (IDIBAPS), 08036 Barcelona, Spain, and [‡‡]Tissue Repair and Regeneration Program, Institute of Health and Biomedical Innovation, Queensland University of Technology, Brisbane, Queensland 4095, Australia*

Annexins are a family of proteins that bind to phospholipids in a calcium-dependent manner. Earlier studies implicated annexin A6 (AnxA6) to inhibit secretion and participate in the organization of the extracellular matrix. We recently showed that elevated AnxA6 levels significantly reduced secretion of the extracellular matrix protein fibronectin (FN). Because FN is directly linked to the ability of cells to migrate, this prompted us to investigate the role of AnxA6 in cell migration. Up-regulation of AnxA6 in several cell models was associated with reduced cell migration in wound healing, individual cell tracking and three-dimensional migration/invasion assays. The reduced ability of AnxA6-expressing cells to migrate was associated with decreased cell surface expression of $\alpha V\beta 3$ and $\alpha 5\beta 1$ integrins, both FN receptors. Mechanistically, we found that elevated AnxA6 levels interfered with syntaxin-6 (Stx6)-dependent recycling of integrins to the cell surface. AnxA6 overexpression caused mislocalization and accumulation of Stx6 and integrins in recycling endosomes, whereas siRNA-mediated AnxA6 knockdown did not modify the trafficking of integrins. Given our recent findings that inhibition of cholesterol export from late endosomes (LEs) inhibits Stx6-dependent integrin recycling and that elevated AnxA6 levels cause LE cholesterol accumulation, we propose that AnxA6 and blockage of LE cholesterol transport are critical for endosomal function required for Stx6-mediated recycling of integrins in cell migration.

After initial evidence from our laboratory and others for a role of the hepatic endocytic compartment in the modulation of ECM[6] (1), it is now well established that endosomes contribute to multiple aspects of cell migration and invasion (2). This complex and multifunctional process requires a plethora of molecules along endo- and exocytic pathways, enabling the delivery of ECM, integrins, and signaling proteins to the cell surface. To orchestrate and coordinate this complexity, involvement of Rab and soluble *N*-ethylmaleimide-sensitive factor attachment protein (SNAP) receptor (SNARE) proteins together with cytoskeleton elements is well documented (3, 4). Furthermore, because cellular movement requires dynamic reorganization of membrane domains, lipids, in particular cholesterol, but also other less well known proteins participate. In this study, we show that a member of the annexin family, AnxA6, and most likely its ability to impact cellular cholesterol transport and distribution, regulate integrin cell surface expression and consequently cell migration.

Annexins are evolutionarily conserved proteins that bind to acidic phospholipids in a calcium-dependent manner and have been described to regulate membrane trafficking events along endo- and exocytic pathways (5). Several reports revealed links between AnxA6 and various aspects of cell migration. First, early studies identified AnxA6 as a potential receptor for fetuin-A and chondroitin sulfate proteoglycans (6–8). Second, we showed that membrane targeting of AnxA6 correlated with

* This work was supported by the Ministerio de Economía y Competitividad (MINECO) Grants BFU2012-36272 and CSD2009-00016 and Fundació Marató TV3 Grant PI042182 (Spain) (to C. E.) and by University of Sydney, Australia Grants U1758 and U7007 (to T. G.). The authors declare that they have no conflicts of interest with the contents of this article.

[1] These authors contributed equally to this work.

[2] Present address: University of Bonn, Pharmaceutical Institute, Pharmaceutical Chemistry I, D-53121 Bonn, Germany.

[3] To whom correspondence may be addressed: Dept. de Biologia Cel·lular, Immunologia i Neurociències, Facultat de Medicina, Universitat de Barcelona, 08036 Barcelona, Spain. Tel.: 34-934021908; Fax: 34-4021907; E-mail: enrich@ub.edu.

[4] To whom correspondence may be addressed. Tel.: 612-9351-8496; Fax: 612-9351-4391; E-mail: thomas.grewal@sydney.edu.au.

[5] Supported by CONSOLIDER-INGENIO (MINECO) Research Program Postdoctoral Fellowship Grant CSD2009-00016 and Fundació Marató TV3. To whom correspondence may be addressed: Dept. de Biologia Cel·lular, Immunologia i Neurociències, Facultat de Medicina, Universitat de Barcelona, 08036 Barcelona, Spain. Tel.: 34-934021908; Fax: 34-4021907; E-mail: carles.rentero@ub.edu.

[6] The abbreviations used are: ECM, extracellular matrix; AnxA6, annexin A6; CTxB, cholera toxin B; FAK, focal adhesion kinase; FN, fibronectin; KD, knockdown; LE, late endosome; NPC, Niemann-Pick type C; SNAP, soluble *N*-ethylmaleimide-sensitive factor attachment protein; Stx, syntaxin; RE, recycling endosome; STxB, shiga toxin B; TGN, *trans*-Golgi network; VAMP, vesicle-associated membrane protein; EGFR, epidermal growth factor receptor; sulfo-NHS-SS-biotin, *sulfosuccinimidyl-2-(biotinamido)ethyl-1,3′-dithiopropionate; Tf, transferrin;* Tf-R, transferrin receptor; CHO, Chinese hamster ovary cell; FCS, fetal bovine serum; HBSS, Hanks' buffered salt solution.

the stabilization of the cortical actin cytoskeleton (9). Third, reduced AnxA6 expression appeared to contribute to breast cancer progression by promoting the loss of functional cell-cell and/or cell-ECM contacts (10). Fourth, the scaffolding function of AnxA6 may alter the activity of receptors, such as the epidermal growth factor receptor (EGFR) and downstream effector pathways, including the Ras/mitogen-activated protein kinase (MAPK) signaling cascade, which are well known to contribute to cancer cell motility and invasiveness (11–13). Finally, we recently identified that elevated levels of AnxA6 cause a Niemann-Pick type C1 (NPC1)-like phenotype, which is characterized by an accumulation of cholesterol in LEs. This was associated with reduced caveolin transport to the cell surface but also mislocalization of several SNARE proteins, including SNAP23 and Stx4 (14, 15). Both SNAP23 and Stx4 are normally engaged in the delivery of secretory vesicles to the cell surface; however, their mislocation upon AnxA6 overexpression inhibited exocytic pathways, including FN secretion (15).

Cholesterol is considered indispensible for cell migration. The activity of Rac/Rho GTPases, which drive cellular movement, is sensitive to cholesterol levels and distribution in the plasma membrane (16). Similarly, cholesterol depletion using statins interferes with the invasive morphology of breast cancer cells (17). Recruitment of integrins to focal adhesions for cell migration requires cholesterol (18, 19). Endocytosed LDL cholesterol from LEs controls the formation of focal adhesions at the leading edge of cells (20). Overall, dietary, genetic, and pathological changes in cholesterol metabolism seem to affect the migratory behavior of cancer cells (21–23). Hence, we hypothesized that AnxA6-induced alterations in the cellular distribution of cholesterol could be an additional mechanism affecting cell motility.

The present study shows for the first time how elevation of AnxA6 levels interferes with cell migration. Mechanistically, this is caused by LE cholesterol accumulation in AnxA6-expressing cells, which leads to the mislocalization of Stx6, a SNARE protein that is essential for the cell surface delivery of integrins.

Experimental Procedures

Reagents and Antibodies—Nutrient mixture Ham's F-12 and DMEM were from Biological Industries. Hanks' buffered salt solution (HBSS) was from Gibco. FN, filipin, saponin, L-glutathione, poly-L-lysine, protein G-Sepharose, U18666A, water-soluble cholesterol, and iodoacetamide were from Sigma. Paraformaldehyde was from Electron Microscopy Sciences, and Mowiol was from Calbiochem. Sulfo-NHS-SS-biotin and streptavidin beads were from Fisher Scientific. Polyclonal anti-AnxA6 was prepared in our laboratory and has been described elsewhere (24, 25). Polyclonal anti-human integrin β1 and mouse IgG1 (κ isotype) were from BioLegend. Monoclonal anti-αV, -α5, and -β3 integrins; anti-GM130; anti-Stx6; and rat IgG2a (κ isotype) were from BD Biosciences. Polyclonal anti-αV and monoclonal anti-α5 (PB1) integrins were from Millipore and the Developmental Studies Hybridoma Bank (The University of Iowa), respectively. Monoclonal anti-actin was from MP Biomedicals, anti-transferrin receptor (Tf-R) and horseradish peroxidase-conjugated secondary antibodies were from Zymed Laboratories Inc. Polyclonal anti-VAMP3 (Cellubrevin), anti-VAMP4, and anti-Vti1a were from Synaptic Systems. Anti-cation-independent mannose 6-phosphate receptor was from Abcam. Alexa Fluor-conjugated secondary antibodies were from Molecular Probes. Fluorescent cholera toxin B (CTxB; A647-conjugated) was from Molecular Probes. Fluorescent shiga toxin B (STxB) was kindly provided by Dr. Ludger Johannes (Curie Institute, Paris, France). Fluorescent transferrin (Tf-A488) was from Invitrogen. The enhanced green fluorescent protein-tagged AnxA6 expression vector has been described elsewhere (12, 14). Expression vectors encoding NPC1-GFP and NPC1-P692S-GFP were kindly provided by Dr. Matthew P. Scott (Stanford University, Stanford, CA).

Cell Culture, DNA Constructs, and Transfections—Chinese hamster ovary wild-type cells (CHO-WT) and AnxA6-overexpressing CHO (CHO-A6) cells were grown in Ham's F-12 with 10% fetal calf serum (FCS), 2 mM L-glutamine, 100 units/ml penicillin, and 100 μg/ml streptomycin at 37 °C, 5% CO_2. A431-WT, AnxA6-overexpressing A431 (A431-A6), COS-1, HeLa, HeLa-A6KD, and MDA-MB-231 cells were grown in DMEM and supplements as above. The generation of stable CHO-A6 and A431-A6 cell lines and the HeLa cell line with stable AnxA6 knockdown has been described in detail (15, 25). For transient transfections, cells at 50% confluence were transfected with 0.8 μg of DNA/ml using Effectene (Qiagen) or Lipofectamine-LTX (Invitrogen) following the manufacturers' instructions. For Stx6, Stx4, and AnxA6 knockdown studies, cells (70% confluence) were transfected with siRNA (100 μM) targeting mouse Stx6 (5′-GGAUUGUUUCAGAGAUGGAtt-3′, 5′-GGACCUCGAUGAAACCAUCtt-3′, and 5′-GGAUCAGAUGUCAGCUUCAtt-3′) and Stx4 (5′-GGAAGCUGAUGAGAAUUACtt-3′) (Ambion BioSciences) and human and mouse AnxA6 (Santa Cruz Biotechnology, sc-29688 and sc-29689) with Lipofectamine 2000 according to the manufacturer's instructions. Studies were conducted after 72 h. Scrambled siRNA served as a negative control (5′-GGAATCTCATTCGATGCATAC-3′). In some experiments, cells were treated with U18666A as described previously (15, 24).

Immunoprecipitation—Cells were grown on 100-mm dishes, washed with PBS, and solubilized in TGH buffer (1% Triton X-100, 10% glycerol, 50 mM NaCl, 50 mM HEPES, pH 7.3, 1 mM Na_3VO_4, 10 mM NaF, 1 mM PMSF, 10 mg/ml leupeptin, 10 mg/ml aprotinin) followed by centrifugation at 12,000 × *g* for 10 min at 4 °C. Proteins from supernatants (500 – 800 μg) were incubated with 2 μg of mouse monoclonal anti-Stx6, rabbit polyclonal anti-VAMP4, or mouse/rabbit IgG for 2 h at 4 °C, respectively, followed by an additional 60-min of incubation upon addition of protein G-Sepharose. Immunoprecipitates were washed twice in TGH containing 150 mM NaCl and once in TGH without NaCl and analyzed for Stx6, VAMP3, Stx16, VAMP4, and Vti1a (15).

Microscopic Techniques and Image Analysis—Cells were grown on coverslips, fixed with 4% paraformaldehyde for 20 min, washed, permeabilized with 0.1% saponin for 10 min, blocked with 1% BSA for 5 min, and incubated with primary and secondary antibodies. Alternatively, cells were permeabilized with 0.1% Triton X-100 for 5 min. In some experiments, cells were seeded onto FN-coated coverslips; therefore cover-

slips were washed twice with PBS, coated with poly-L-lysine (50 μg/ml) in PBS for 2 h, washed twice with PBS, incubated in 20 μg/ml FN for 3 h, and washed twice with PBS before use. Finally, samples were mounted in Mowiol, and cells were observed using a Leica DMI 6000B epifluorescence inverted microscope equipped with an HCX PLA Apo 63× oil immersion objective. Some images were captured with a Leica TCS SP5 laser scanning confocal microscope equipped with a DMI6000 inverted microscope, blue diode (405 nm), argon (458/476/488/496/514 nm), diode-pumped solid state (561 nm), HeNe (594/633 nm) lasers, and Apo 63× oil immersion objective lenses. Image analysis was performed with NIH ImageJ software (26). Co-localization analysis was done using the ICA (intensity correlation analysis) plug-in. To quantify staining intensity, images were captured using identical microscope settings.

Isolation of Subcellular Fractions—Subcellular fractionation of CHO-WT and CHO-A6 membranes on discontinuous sucrose gradients was performed, and the distribution of Stx6, RE (VAMP3), *trans*-Golgi network (TGN)-Golgi (Golgin-97), and plasma membrane markers (Na^+/K^+-ATPase) was analyzed. The cholesterol content (percentage of total cellular cholesterol) of each fraction from both cell lines was determined using the Amplex™ Red Cholesterol Assay kit (Molecular Probes) according to the manufacturer's instructions. Subcellular fractionation procedures for the isolation of Golgi membranes from CHO cells have been described in detail previously (27).

Biotinylation and Recycling Assays for Integrins—Cells were washed in HBSS, incubated with sulfo-NHS-SS-biotin (0.15 mg/ml for 10 min), and then washed with HBSS, 5 mM Tris. Cells were lysed and centrifuged at 14,000 × *g* for 20 min at 4 °C. Equal amounts of protein from the supernatant were incubated for 1 h with streptavidin beads to precipitate biotinylated proteins, which were analyzed by immunoblotting.

Integrin recycling was measured as described previously (28). In brief, cell surface biotin-labeled cells were incubated for an additional 30 min to allow internalization of surface biotinylated proteins (quadruplicates for each cell line). One plate was lysed, whereas the three other plates were washed twice in HBSS followed by two washes in PBS, 0.5 mM EDTA. The remaining surface biotin was removed by incubating cells with reduced L-glutathione buffer (50 mM reduced L-glutathione, 75 mM NaCl, 2 mM EDTA, 75 mM NaOH, 0.1% BSA). Reduced L-glutathione was neutralized with 10 mM iodoacetamide in HBSS. Cells from a second plate were then lysed, and the remaining two plates were incubated for 30 min in complete cell culture medium. One plate was lysed, whereas the other plate was incubated with reduced L-glutathione and iodoacetamide as described above to remove the surface biotin from recycled proteins.

Multiscratch Assays—Multiscratch signaling assays were performed as described (29). In brief, 5×10^5 cells were seeded onto 6-well plates and grown to 90% confluence. Using a 200-μl pipette tip, five vertical and five horizontal scratches were made, and lysates were prepared at 0, 30, and 60 min postscratch. Cell lysates were analyzed by Western blotting for total and phosphorylated ($Tyr(P)^{861}$) focal adhesion kinase (FAK) and ($Tyr(P)^{527}$) Src.

CTxB and STxB Uptake—Cells were incubated in DMEM, 10% FCS with fluorescently labeled CTxB and STxB (CTxB-Cy5, 2 μg/ml; STxB-Cy3, 1 μg/ml) for 10 min at 37 °C. Non-internalized CTxB and STxB was removed, and cells were incubated for an additional 5–60 min before fixation.

Internalization of α5 Integrin—CHO cells were plated on FN-coated coverslips (20 mg/ml) for 24 h followed by incubation with α5 integrin antibody (PB1) (diluted 1:100 in complete Ham's F-12) for 1 h at 4 °C to allow the antibody to bind cell surface α5 integrin. Then samples were washed with pre-warmed medium and incubated for 1 h at 37 °C to allow internalization of antibody-labeled α5 integrin. Cells were washed with PBS, fixed, and immunostained as described above.

Cell Tracking Assays—Cells were seeded on FN-coated plates (10 μg/ml for A431 and 20 μg/ml for CHO cells). Migration was monitored by time lapse video microscopy, and bright field images were acquired at a rate of 10 min/frame for 14 h. Cell migration (velocity) was measured using MtrackJ (ImageJ) (30).

Organotypic Invasion Assay—7.5×10^4/ml primary human fibroblasts were embedded in three-dimensional matrices of rat tail collagen type I. Rat tail tendon collagen solution was prepared by the extraction of tendons with 0.5 M acetic acid (≈2 mg/ml). Detached, polymerized matrix (2.5 ml) in 35-mm dishes was allowed to contract for 6 days in DMEM, 10% FCS until fibroblasts had contracted the matrix to ≈1.5-cm diameter (31). Then 4×10^4 A431-WT and A431-A6 cells were plated on top of the matrix in complete medium and allowed to grow to confluence for 5 days. The matrix was then mounted on a metal grid and raised to the air/liquid interface, resulting in the matrix being fed from below with complete medium that was changed every 2 days. After 12 days, the cultures were fixed using 4% paraformaldehyde and processed for hematoxylin and eosin (H&E) staining. The invasion index was calculated as the percentage of cells that invaded beyond ≈30 μm as a percentage of total cells in the assay.

Matrigel Migration/Invasion Assay—Cell invasion was analyzed using BD BioCoat Matrigel invasion chambers with 8-μm-pore size polyethylene terephthalate membrane inserts according to the manufacturer's protocol (BD Biosciences). Briefly, 6×10^4 cells per insert were seeded on the upper chamber in serum-free medium. The lower chamber contained DMEM supplemented with 10% FCS as chemoattractant. After 72 h at 37 °C, cells remaining in the upper chamber were removed. Cells that had invaded the lower chamber were fixed and stained with Diff-Quick stain (Lab Aids, Australia). As a control, migration on uncoated inserts was determined. Images were captured using a Nikon Eclipse TS100 microscope.

Wound Healing Assays—Six-well plates were marked with horizontal lines at the base of the plate. 5×10^5 CHO-WT, CHO-A6, A431-WT, and A431-A6 cells were seeded in triplicate and grown until ~70% confluence. A scratch, using the tip of a P10 pipette, was then made across the center of each well such that the scratch was perpendicular to the marked horizontal lines. Images were acquired immediately after scratching ($t = 0$) and postscratch at $t = 4$, 8, 12, 16, 24, 48, and 60 h, respectively, until cells completely covered the scratched area.

Cells were washed at each time point to remove possible cell debris and non-adherent cells. Scratches were studied at 10× magnification using a Nikon Eclipse TS100 inverted microscope, and images were collected with Leica Microsystems Digital Imaging. Image analysis was performed with ImageJ software. The area of the scratch was calculated for the various time points as percent reduction in area over time. Three independent experiments in triplicate per cell line were performed.

Flow Cytometry—Cells were harvested in PBS, 0.5 mM EDTA; resuspended in ice-cold PBS, 1% FCS (FACS buffer); and incubated in FACS buffer with anti-integrins (0.01 μg/ml α5 and β3; 0.02 μg/ml αV) for 1 h. Cells were washed, incubated with fluorescently tagged secondary antibody for 1 h, and then washed again. Cell surface fluorescence was measured using FACS-CantoII cytometer at 4 °C.

Statistics—Error bars depict standard deviation (S.D.). Statistical significance was determined with GraphPad Prism by unpaired Student's *t* test or analysis of variance test as indicated (*, $p < 0.05$; **, $p < 0.01$; ***, $p < 0.001$).

Results

Elevated AnxA6 Levels Reduce Cell Migration and Invasion—The reduced FN secretion in cells with high levels of AnxA6 (15) prompted us to examine cell migration. Two cell models were mainly used in this study: A431 cells (A431-WT), which lack endogenous AnxA6, and A431 cells stably overexpressing AnxA6 (A431-A6) and CHO-WT *versus* CHO-A6, both described extensively in previous studies (25, 32). AnxA6 levels in the CHO-A6 and A431-A6 cell line are comparable with endogenous AnxA6 levels in other commonly used epithelial cell lines, such as NRK and HeLa (data not shown). In addition, the calcium- and cholesterol-regulated distribution of endogenous and ectopically expressed AnxA6 at the plasma membrane and the endosomal compartment is comparable (11, 12, 15, 24, 25, 27), making these cell lines suitable for further studies.

We first compared cell migration in wound healing assays. In both cell lines stably overexpressing AnxA6, wound closure was significantly slower compared with their wild-type counterparts (Fig. 1, *A* and *D*; quantification in *B* and *E*). In addition, we compared the movement of individual cells using time lapse video microscopy and by manually marking the speed and direction of individual cell migration tracks. In both A431 and CHO cells stably expressing AnxA6, the velocity was significantly lower compared with the controls (Fig. 1, *C* and *F*). In A431-A6 cells, this also correlated with an increased directionality index (distance/trajectory index) (data not shown).

Next, using Transwell Matrigel invasion chambers (see "Experimental Procedures"), large numbers of A431-WT cells migrating/invading toward a chemoattractant (FCS) were observed (Fig. 1*G*). In contrast, A431-A6 cells exhibited reduced migration and a dramatic decrease (7.3-fold) in their capacity to invade (see also quantification in Fig. 1*G*).

To assess the invading properties of cells ±AnxA6 in an *in vivo* like setting, we then compared invasiveness of A431-WT and A431-A6 cells in three-dimensional organotypic matrices that more closely recapitulate a tumor stromal environment (31). A431-WT cells moved into organotypic matrices in considerable numbers over a 12-day period (Fig. 1*H*, including quantification on the *right*). By contrast and after normalization to cell number, invasion of A431-A6 cells into the three-dimensional organotypic matrices was significantly reduced by 50 ± 3%.

As proof of concept, we compared migration and invasion in HeLa, which express substantial amounts of AnxA6, and the AnxA6-depleted HeLa cell line (HeLa-A6KD) (11). HeLa-A6KD cells displayed ≈ 4-fold increased migration/invasion and a 45–55% elevated invasion index compared with controls (Fig. 1*I*). Finally, the MDA-MB-231 breast cancer cell line, a well established model to examine aggressive metastatic cell behavior, was analyzed. MDA-MB-231 express significant amounts of AnxA6 (12), and AnxA6 depletion in MDA-MB-231 cells using RNAi knockdown increased wound closure by ~20% compared with controls (data not shown).

Finally, to correlate reduced migration in A431-A6 cells with cellular signaling, we analyzed the activity of key players in integrin signaling and cell migration, FAK and Src kinase. FAK and Src activation is complex with Src-mediated phosphorylation of FAK at tyrosine 861 (Tyr(P)^{861}-FAK) being essential to promote focal adhesion assembly (33). Increased Src activity correlates with reduced phosphorylation of the autoinhibitory Tyr^{527} residue (Tyr(P)^{527}-Src) (34).

Multiscratch wound healing assays (29) were performed, and cell lysates prepared at $t = 0$, 30, and 60 min postscratch were analyzed for Tyr(P)^{861}-FAK and Tyr(P)^{527}-Src phosphorylation. Although A431-WT cells displayed elevated Tyr(P)^{861}-FAK levels and reduced Tyr(P)^{527}-Src levels postscratch, consistent with the activation of the signaling machinery required for cell migration during wound closure, A431-A6 cells showed decreased Tyr(P)^{861}-FAK and increased Tyr(P)^{527}-Src (Fig. 1*J*), which correlated with reduced motility and invasiveness in migration/invasion assays (Fig. 1, *A–C*, *G*, and *H*). Thus, manipulation of AnxA6 levels in different cell lines modulates migration and invasion, indicating a general role for AnxA6 levels in this process.

Integrin Recycling Is Reduced in AnxA6-overexpressing Cells—Recycling of integrins is crucial for cell migration (19, 35). Integrins consist of α and β subunits that bind ECM proteins to regulate cell adhesion and migration (36). Consistent with the reduced migratory ability of cells with up-regulated AnxA6 levels (Fig. 1), flow cytometry identified the significant diminution of cell surface αV, β3, and α5 integrins in CHO-A6 cells, in particular in cells plated onto FN (Fig. 2*A*).

To substantiate these findings, cell surface expression of biotinylated integrins was analyzed (Fig. 2*B*). In line with the above studies, reduced cell surface expression of αV (60.7 ± 12.9%) and α5 (78.2 ± 7.6%) integrins was observed in CHO-A6 cells (Fig. 2*B*, *lanes 1* and *2*), whereas total integrin levels were comparable in both cell lines (compare *lanes 3* and *4*).

In support of these findings, α5 integrin was mainly localized at the plasma membrane in CHO-WT (see *arrowheads*) but accumulated in the perinuclear region of CHO-A6 cells (Fig. 2*C*). In line with Rab11 regulating β1 integrin recycling (37), these intracellular pools of α5 co-localized with Rab11-GFP and VAMP3 (see *dashed squares* and *insets*), suggesting that reduced α5 integrin cell surface expression in AnxA6-express-

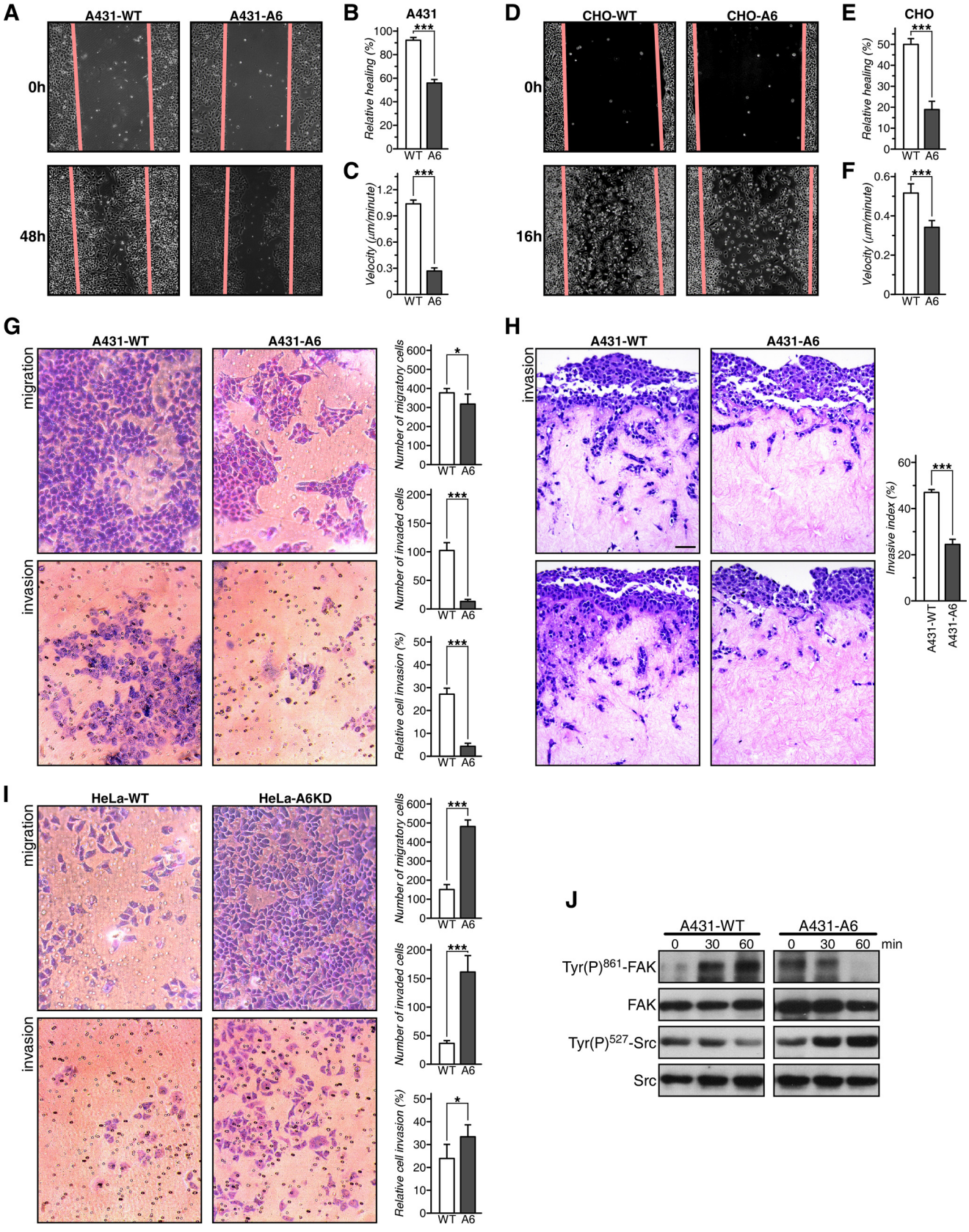
A
A431-WT
A431-A6
0h
48h
B
A431
Relative healing (%)
WT A6
C
Velocity (μm/minute)
D
CHO-WT
CHO-A6
16h
E
CHO
F
G
migration
invasion
Number of migratory cells
Number of invaded cells
Relative cell invasion (%)
H
Invasive index (%)
I
HeLa-WT
HeLa-A6KD
J
Tyr(P)861-FAK
FAK
Tyr(P)527-Src
Src
min

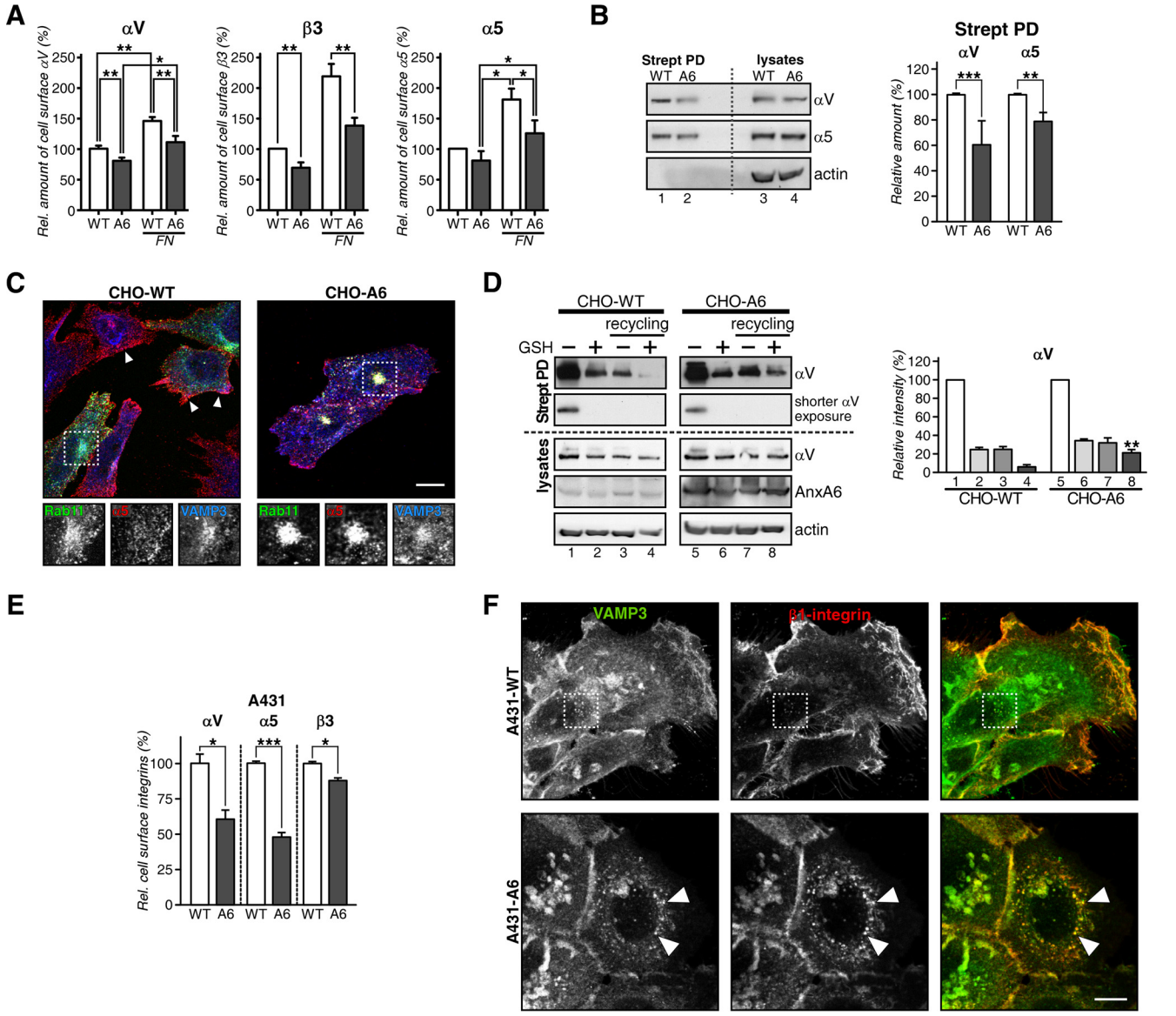

FIGURE 2. **Reduced cell surface expression of integrins in AnxA6-overexpressing cells.** *A*, cell surface expression of αV, β3, and α5 integrins determined by flow cytometry of CHO-WT (*WT*) and CHO-A6 (*A6*) cells ±FN. Values were normalized to CHO-WT. *B*, total (*lysates*) and cell surface biotinylated (*Strept PD*) αV and α5 integrins from CHO-WT and CHO-A6 cells. *C*, co-localization of α5 integrin with Rab11-GFP and VAMP3 in CHO-WT and CHO-A6 cells. *Arrowheads* point to α5 integrin at the plasma membrane in CHO-WT cells. Co-localization of Rab11-GFP, α5 integrin, and VAMP3 in CHO-A6 cells is indicated (see *dashed square*). *Scale bar*, 10 μm. *D*, αV integrin recycling in CHO-WT (*lanes 1–4*) and CHO-A6 (*lanes 5–8*) cells. A shorter exposure of the same experiment is also shown. Biotin-labeled αV integrins at the cell surface (*lanes 1* and *5*), internalized after 30 min (*lanes 2* and *6*) and total internalized-recycled pool (*lanes 3* and *7*) and in the recycling compartment (*lanes 4* and *8*) were quantified (**, $p < 0.01$; two independent experiments). Total αV, AnxA6, and actin from each lysate are shown. *E*, cell surface expression of αV, α5, and β3 integrins determined by flow cytometry in A431-WT and A431-A6 cells. *F*, immunolabeling of β1 integrin with VAMP3 in A431-WT and A431-A6 cells. *Arrowheads* point to β1 integrin/VAMP3 co-localization in the perinuclear region of A431-A6 cells. *Scale bar*, 10 μm. *, $p < 0.05$; ***, $p < 0.001$. *Error bars* shown in the figure represent S.D.

FIGURE 1. **AnxA6 overexpression reduces cell migration and invasion.** *A* and *D*, wound closure of A431-WT (*WT*) and A431-A6 (*A6*) cells (*A*) and CHO-WT and CHO-A6 cells (*D*). The relative percentage of wound closure was calculated (*B* and *E*). Data represent the mean ± S.E. from three independent experiments done in triplicate. Representative images of cell migration are shown. A431-WT and A431-A6 (*C*) and CHO-WT and CHO-A6 cells (*F*) were plated on FN, and movement of cells was recorded by time lapse video microscopy for 12 h. Individual cell migration tracks were marked, and the speed (velocity) was recorded and quantified. *G*, Transwell migration and invasion of A431-WT and A431-A6 cells. Representative images from two independent experiments with duplicate samples are shown. Migrating and invading cells from six fields per cell line were quantified, and relative invasion was calculated. *H*, organotypic invasion assay with A431-WT and A431-A6 cells plated on three-dimensional matrices of rat tail collagen. Cells were allowed to invade for 12 days, fixed, and processed for H&E staining. The invasion index was calculated as the percentage of total cells (14,506 cells) that invaded beyond ≈30 μm. Representative images of three independent experiments are shown. *Scale bar,* 10 μm. *I*, Transwell migration and invasion of HeLa and HeLa-A6KD cells. Representative images from two independent experiments with duplicate samples are shown. Migrating and invading cells from six fields per cell line were quantified, and relative invasion was calculated. *J*, multiscratch signaling assays were performed as described (29). Cell lysates were prepared at $t = 0$, 30, and 60 min postscratch and analyzed by Western blotting for total and phosphorylated (Tyr(P)^{861}) FAK and (Tyr(P)^{527}) Src as indicated. *, $p < 0.05$; ***, $p < 0.001$. *Error bars* shown in the figure represent S.E.

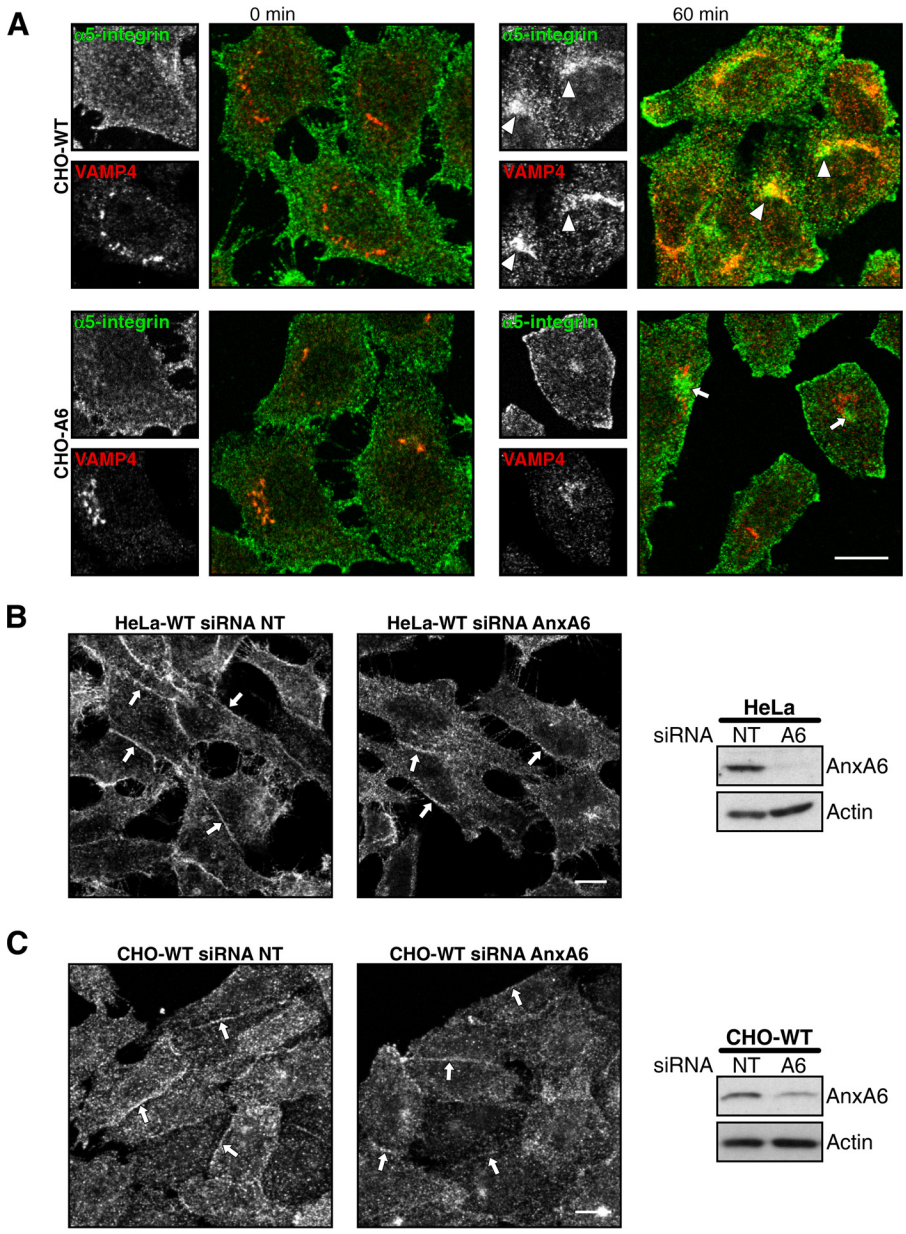

FIGURE 3. **siRNA-mediated AnxA6 knockdown does not interfere with integrin trafficking in CHO and HeLa cells.** *A*, endocytosed α5 integrin traffics to the VAMP4 compartment in CHO-WT cells. Cell surface α5 integrin was tagged by incubation with a monoclonal antibody at 4 °C, and internalization was stimulated at 37 °C for 60 min. *Arrowheads* point to integrin accumulation in the TGN (VAMP4; *red*) in CHO-WT cells; *small white arrows* point to α5 integrin in the recycling compartment in CHO-A6 cells. *B* and *C*, HeLa (*B*) and CHO-WT cells (*C*) were analyzed for the cellular distribution of α5 integrin upon AnxA6 knockdown (*siRNA A6*). Scrambled non-targeting siRNA (*siRNA NT*) served as a control. In control and AnxA6-depleted cells, α5 integrin was mostly located at the plasma membrane (including adjacent and limiting membranes; see *arrows*). *Right panels* in *B* and *C* show Western blot analysis of AnxA6 expression and actin as a control of loading. *Scale bars*, 10 μm.

ing CHO cells was due to its accumulation in the RE compartment.

Finally, we biotinylated the cell surface of CHO-WT and CHO-A6 cells (Fig. 2*D*, *lanes 1* and *5*) followed by internalization of biotin-labeled integrins for 30 min. Then surface biotin-labeled integrins were removed (*lanes 2* and *6*), and cells were allowed to recycle the internal pool of biotinylated αV integrin (*lanes 3* and *7*) (28). Almost all αV integrin reappeared at the cell surface of CHO-WT cells (*lane 8*), whereas in CHO-A6 cells, ≈20% of biotinylated αV remained in the recycling compartment (*lane 4*). Hence, up-regulation of AnxA6 interferes with αV integrin recycling. Similarly, integrin surface expression was reduced (Fig. 2*E*), and β1 integrin accumulated in the VAMP3-positive recycling compartment of A431-A6 cells (Fig. 2*F*).

Because α3 integrin recycling to the cell surface involves trafficking through the TGN in HeLa cells (38), we determined whether α5 integrin also recycles through the VAMP4-containing TGN compartment of CHO cells. Fig. 3*A* shows that a population of α5 integrin co-localizes with VAMP4 after 60 min of antibody internalization in CHO-WT (see *arrowheads*) but not in CHO-A6 cells. Thus, recycling trafficking routes of integrins through TGN compartments appear disrupted upon elevation of AnxA6 levels. Given the dose-dependent manner how

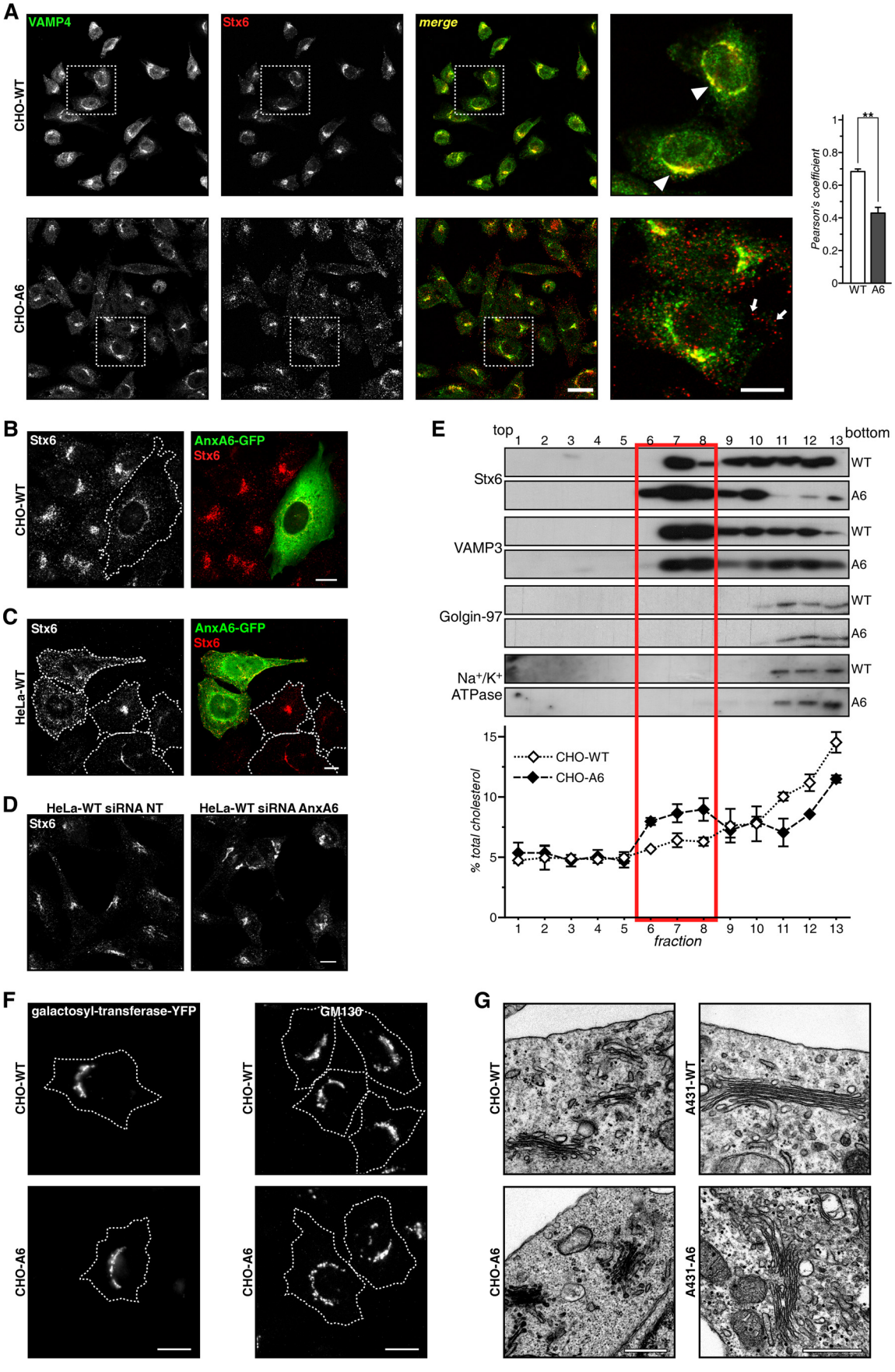
A
VAMP4
Stx6
merge
CHO-WT
CHO-A6
Pearson's coefficient
**
WT A6
B
Stx6
AnxA6-GFP
Stx6
CHO-WT
C
Stx6
AnxA6-GFP
Stx6
HeLa-WT
D
HeLa-WT siRNA NT
HeLa-WT siRNA AnxA6
Stx6
E
top
bottom
Stx6
VAMP3
Golgin-97
Na+/K+ ATPase
WT
A6
CHO-WT
CHO-A6
% total cholesterol
fraction
F
galactosyl-transferase-YFP
GM130
CHO-WT
CHO-A6
G
CHO-WT
A431-WT
CHO-A6
A431-A6

AnxA6 interfered with integrin surface expression, we hypothesized that AnxA6 depletion would not alter the cellular distribution of integrins. Indeed, upon siRNA-mediated AnxA6 knockdown in HeLa (Fig. 3*B*) or CHO wild-type cells (Fig. 3*C*), we did not observe any significant changes in cholesterol distribution as judged by filipin staining (data not shown), and in line with this observation, the membrane staining pattern of α5 integrin was comparable with siRNA non-targeting control counterparts.

Stx6 Distribution in AnxA6-overexpressing Cells—We and others have shown that recycling of endocytosed integrins, such as $\alpha V\beta 3$ and $\alpha 5\beta 1$, requires Stx6 and determines cell surface integrin levels (28, 38–40). Therefore, we investigated whether the overexpression of AnxA6 perturbed Stx6 expression and/or subcellular distribution.

Stx6 is mainly found in the TGN and shuttles to endocytic compartments for TGN or post-Golgi trafficking events (41, 42). In CHO-WT cells, Stx6 was located in perinuclear TGN structures and limited scattered vesicles with the majority of Stx6-positive structures co-localizing with the Golgi marker VAMP4 (Fig. 4*A*) (or TGN46; not shown). In contrast, in CHO-A6 cells, Stx6 was predominantly observed in punctate vesicular structures (see quantification of co-localization in Fig. 4*A*). A similar vesicular Stx6 staining was detected after transient AnxA6-GFP expression in CHO-WT (Fig. 4*B*). Similar patterns of labeling were also observed in HeLa cells upon ectopic GFP-AnxA6 expression (Fig. 4*C*) as well as in A431-A6 (not shown) but not in the siRNA AnxA6-depleted HeLa cells (11) (Fig. 4*D*).

Then the distribution of Stx6 and compartment-specific markers (VAMP3, Golgin-97, and Na^+/K^+-ATPase) in gradients designed to separate endosomes from plasma membrane (Fig. 4*E*) was compared. The TGN and REs are not clearly separated in CHO cells (43), and consistent with the microscopy (Fig. 4*A*), Stx6 was enriched in lighter membrane fractions (fractions 6–8) in CHO-A6 cells, which contain high amounts of RE marker (VAMP3). As shown previously (14), cholesterol levels in Golgi and plasma membrane fractions (fractions 11–13) of CHO-A6 cells were reduced. Despite the drastic dispersion of Stx6 in vesicular structures, Golgi morphology was not affected upon ectopic AnxA6 expression in CHO and A431 cells as evidenced by the comparable distribution of several Golgi markers, such as galactosyltransferase-YFP, GM130, and others (giantin and Stx16; data not shown), as well as the morphological characterization of the Golgi apparatus by electron microscopy (Fig. 4, *F* and *G*).

Stx6 has been identified in early endosomes (44), but very little co-localization was observed between Stx6 and EEA1 (early endosomes), Rab4-GFP (early RE compartment), and Rab7 and Rab9 (LE) in CHO cells (data not shown). However, in CHO-A6 cells, Stx6 clearly co-localized with RE markers Rab11-GFP and VAMP3 (45) (Fig. 5*A*, see *dashed squares* and *arrowheads* in enlarged *insets* and quantification of co-localization in the *right panel*). The same redistribution of Stx6 was observed in A431-A6 cells (Fig. 5*B*).

To assess whether Stx6 mislocalization upon AnxA6 up-regulation would be associated with overall dysregulation of trafficking at the Golgi-endosome interface, we examined retrograde transport. During retrograde transport, Stx6 shuttles between the TGN and endocytic compartments (46) and internalization of CTxB and STxB was therefore analyzed as paradigms for this pathway. CTxB internalization was similar in COS-1 cells ± AnxA6 ($t = 5$ min), and CTxB accumulated in the Golgi independently of AnxA6 overexpression ($t = 60$ min) (Fig. 5*C*). Similarly, STxB was internalized and targeted to the Golgi in HeLa cells overexpressing AnxA6 (Fig. 5*D*). Hence, the retrograde pathway is not impaired in AnxA6-overexpressing cells despite Stx6 missorting to REs. Also, the staining pattern of cation-independent mannose 6-phosphate receptor, which is transported through RE compartments, was similar in CHO-WT and CHO-A6 cells (data not shown). As an additional control, we also analyzed the recycling of Tf and the pattern of Tf-R in CHO-WT and CHO-A6 cells. In line with our previous data (25), alterations of Tf recycling kinetics were not observed (data not shown).

Blockage of Cholesterol Export from LE Induces Relocation of Stx6 to RE—Based on the LE cholesterol-sensitive localization observed for several SNAREs, including Stx6, shown recently (15, 40), we hypothesized that inhibition of cholesterol export from LE in AnxA6-overexpressing cells could selectively impair the association of Stx6 with Golgi membranes and trigger Stx6 relocation to REs.

We therefore analyzed the localization of Stx6 in U18666A-treated CHO-WT cells. U18666A is a lysosomotropic tertiary amine that inhibits cholesterol export from LEs/lysosomes, inducing LE cholesterol accumulation similar to NPC mutations (47). Clearly, U18666A triggered the formation of filipin-stained enlarged LEs, which in line with Fig. 6*A* did not co-localize with Stx6. Furthermore, the TGN staining pattern of Stx6 in CHO-WT was not apparent, indicating disassembly of Stx6 from the TGN to cytoplasmic vesicles upon U18666A treatment. Similar findings were obtained from A431 cells (data not shown). Indeed, in CHO-WT cells, Stx6 vesiculation was initiated at 1 μg/ml U18666A, whereas at 2 μg/ml, Stx6 was almost completely dispersed (Fig. 6*B*).

Consistent with Stx6 accumulating in REs, Stx6 levels were reduced in purified Golgi fractions of CHO-A6 cells (Fig. 6*C*, compare *lanes 1* and *2*). U18666A treatment strongly reduced

FIGURE 4. **Localization of Stx6 in AnxA6-overexpressing cells.** *A*, Stx6 and VAMP4 localization in CHO-WT and CHO-A6 cells. *Enlarged areas* show regions of interest. *Arrowheads* point to co-localization of Stx6 in the TGN of CHO-WT cells. *Arrows* indicate scattered distribution of Stx6 staining in CHO-A6 cells. Quantification of VAMP4/Stx6 co-localization is shown in the *right panel*. **, $p < 0.01$. *B*, ectopic AnxA6-GFP expression induces vesicular Stx6 localization in CHO-WT cells. Characterization of Stx6 localization in HeLa and HeLa-A6KD cells is shown. *C*, AnxA6-GFP and Stx6 (*red*) localization in HeLa cells. *D*, HeLa cells were analyzed for the cellular distribution of Stx6 upon AnxA6 knockdown (*siRNA A6*). Scrambled non-targeting siRNA (*siRNA NT*) served as a control. In control and AnxA6-depleted cells, cellular distribution of Stx6 was comparable. *E*, subcellular fractionation of CHO-WT and CHO-A6 membranes on discontinuous sucrose gradients. Distribution of Stx6, RE (VAMP3), TGN-Golgi (Golgin-97), and plasma membrane markers (Na^+/K^+-ATPase) is shown. The cholesterol content (percentage of total cellular cholesterol) of each fraction from both cell lines is given. Characterization of the Golgi compartment in CHO-WT and CHO-A6 cells is shown. *F*, galactosyltransferase-YFP and GM130 staining of CHO-WT and CHO-A6 cells is shown. *G*, ultrathin sections of CHO-WT, CHO-A6, A431-WT, and A431-A6 cells were analyzed by electron microscopy. *Scale bars*, 10 μm in *B–D* and 0.5 μm in *F*. **, $p < 0.01$. *Error bars* shown in the figure represent S.D.

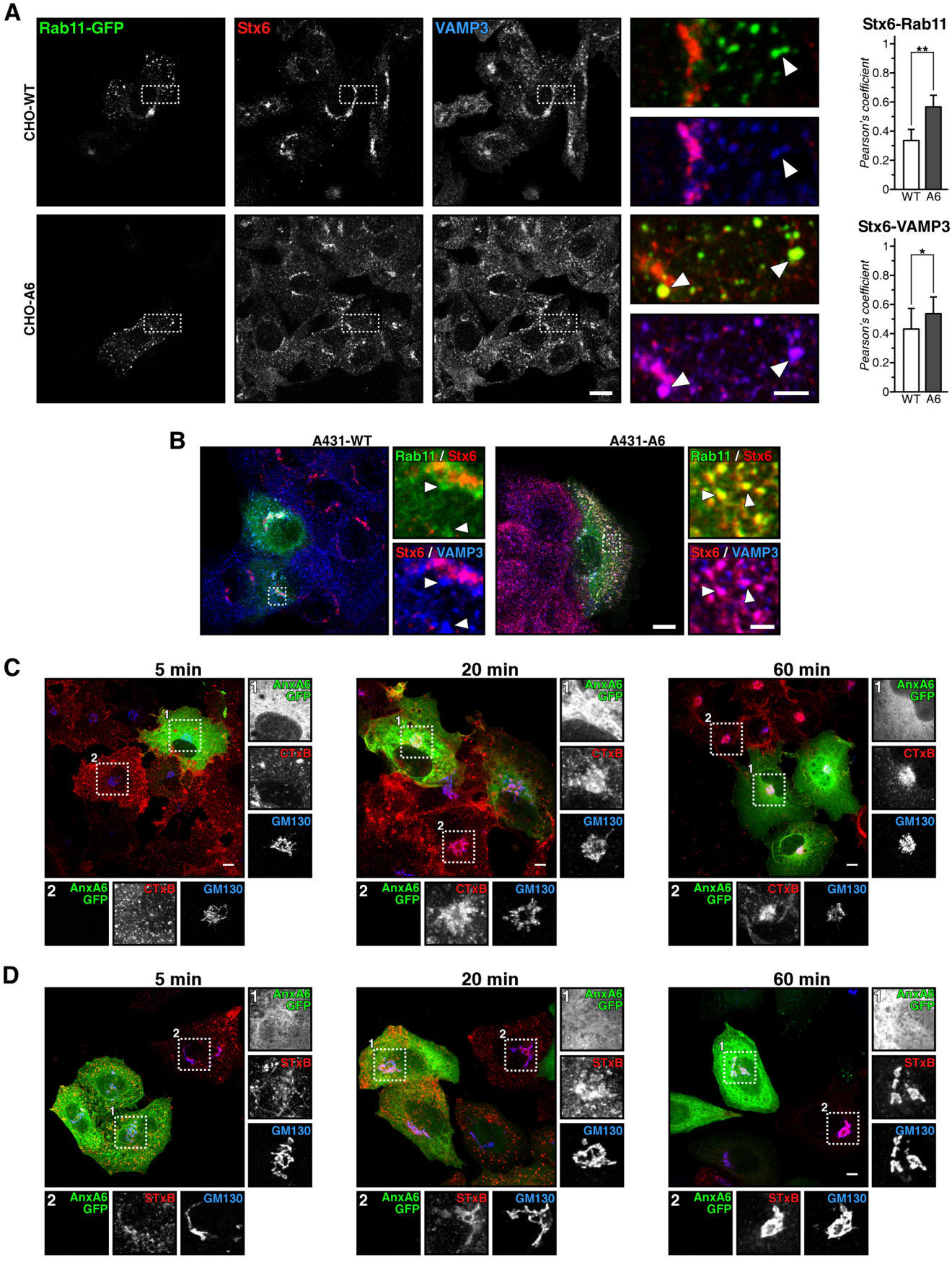
A
Rab11-GFP
Stx6
VAMP3
CHO-WT
CHO-A6
Stx6-Rab11
Pearson's coefficient
1
0.8
0.6
0.4
0.2
0
**
WT
A6
Stx6-VAMP3
Pearson's coefficient
1
0.8
0.6
0.4
0.2
0
*
WT
A6
B
A431-WT
Rab11 / Stx6
Stx6 / VAMP3
A431-A6
Rab11 / Stx6
Stx6 / VAMP3
C
5 min
20 min
60 min
AnxA6 GFP
CTxB
GM130
D
5 min
20 min
60 min
AnxA6 GFP
STxB
GM130

Golgi-associated Stx6 in CHO-WT (compare *lanes 1* and *5*) and even more so in CHO-A6 cells (compare *lanes 2* and *6*), reflecting a significant translocation of Stx6 away from the TGN. Cholesterol levels in Golgi membranes from U18666A-treated CHO-WT and CHO-A6 cells were comparable (Fig. 6*E*). Interestingly, exogenous cholesterol only *lanes 3* and *4*), indicating that different cholesterol pools and routes might determine the association of Stx6 with the Golgi (quantification in Fig. 6*D*).

Stx6 interacts with several SNAREs, including VAMP3, VAMP4, Stx16, and Stx4 (48). Therefore, Stx6 immunoprecipitates from CHO-WT and CHO-A6 cells were compared and analyzed for potential co-precipitation with different SNARE partners. Although VAMP3, Vti1a, and Stx16 co-precipitated with Stx6 to a similar extent in CHO-WT and CHO-A6 cells (Fig. 6, *F*, *G*, and *H*), a significant decrease of Stx6/VAMP4-containing SNARE complexes in CHO-A6 cells was observed (Fig. 6, *F* and the reciprocal immunoprecipitate in *G*). Co-immunoprecipitation of Stx6 with VAMP2, Stx10, or Stx4 was not detected (data not shown). Decreased co-localization of VAMP4/Stx6 in CHO-A6 cells supported these findings (Fig. 4*A*). Importantly, decreased amounts of Stx6-VAMP4 complexes were also observed in U18666A-treated CHO-WT cells (Fig. 6*J*).

AnxA6 induced changes in SNAP23/Stx4 localization without affecting their interaction partners Stx3, VAMP2, VAMP3, and VAMP8 (15). Similarly, expression levels of Stx16, VAMP4, and Vti1a, all SNARE partners of Stx6 in TGN-related endocytic pathways, were comparable in CHO-WT and CHO-A6 cells (Fig. 6*I*).

To investigate whether loss of Stx6 would correlate with reduced cell surface expression of αV and α5 integrins in controls, we silenced Stx6 in CHO-WT cells. These experiments clearly demonstrated Stx6-dependent integrin cell surface expression as αV and α5 cell surface levels were significantly reduced to 65 ± 5 and 20 ± 2.2%, respectively (Fig. 7*A*, compare *lanes 3* and *4*). Up-regulated AnxA6 levels also trigger SNAP23/Stx4 mislocalization (15), and Stx4 can modulate integrin cell surface expression (49). Therefore, we addressed whether Stx4 knockdown in CHO-WT would reduce cell surface integrins. However, 50 ± 8% knockdown of Stx4 depletion did not decrease the surface expression of αV or α5 integrin (Fig. 7*A*, compare *lanes 2* and *4*). Hence, loss of Stx6 in CHO-WT triggered a phenotype comparable with that of the CHO-A6 cell line, strongly indicating that AnxA6 acts through Stx6 as part of the machinery determining cell surface integrin delivery.

In addition, to examine whether reduced integrin cell surface expression could be due to deregulated distribution of cholesterol in CHO-A6 cells; cells were plated onto FN; treated with exogenous cholesterol; surface-immunolabeled with antibodies against α5, αV, and β3 integrins; and analyzed by flow cytometry (Fig. 7*B*). As shown above (Fig. 7*A*; see also Fig. 2), CHO-A6 cells consistently showed reduced cell surface expression of all three integrins. Most remarkably, addition of cholesterol increased cell surface expression of these integrins by 10–20% in CHO-WT cells and even more ($\approx$20–25% for α5) in CHO-A6 cells. However, incomplete recovery in cholesterol-treated CHO-A6 cells suggests additional mechanisms contributing to reduced cell surface integrin expression in these cells.

Finally, to examine whether normalization of cholesterol transport via NPC1 overexpression could rescue AnxA6-mediated inhibition of integrin cell surface expression, NPC1-GFP was ectopically expressed in CHO-A6 cells, and cell surface integrins were analyzed by flow cytometry (Fig. 7*C*) and immunocytochemistry (Fig. 7*D*). NPC1-GFP overexpression restored integrin cell surface expression by 41.6 ± 10.2 (α5), 50.4 ± 2.8 (αV), and 49.4 ± 13% (β3) (Fig. 7*C*). Moreover, NPC1 overexpression robustly reduced the perinuclear accumulation of α5 integrin, which corresponds to the RE compartment (co-localized with transferrin receptor) (Fig. 7*D*), further reinforcing the involvement of LE cholesterol for integrin cell surface expression. In addition, transient overexpression of a loss-of-function NPC1 mutant that cannot bind cholesterol, NPC1-P692S-GFP, in CHO-WT cells reduced cell surface expression of α5, αV, and β3 integrins (Fig. 7*C*). This cholesterol-dependent impairment of integrin delivery to the cell surface seemed to be highly selective because constitutive recycling of other membrane proteins upon AnxA6 expression was not disturbed (*e.g.* Tf-R and EGFR; data not shown). Taken together, our data suggest that inhibition of LE cholesterol export, driven by AnxA6 overexpression, causes reduced cell surface integrin expression via Stx6 mislocalization, which impairs fundamental aspects relevant for cell motility, such as cell migration and invasion in both two- and three-dimensional environments.

Discussion

This study shows that elevated AnxA6 levels triggers Stx6 mislocalization to REs, which is responsible for reduced integrin recycling to the cell surface. Perturbed cholesterol distribution upon AnxA6 up-regulation and our recent studies from NPC1 mutant cells (40) showing that LE cholesterol is critical for Stx6-dependent integrin recycling suggest that elevated AnxA6 levels interfere with integrin trafficking through impaired LE cholesterol export. In support of this hypothesis, ectopic expression of NPC1 restores cell surface integrin expression in cells with high AnxA6 levels. These findings correlate with decreased cell migration and invasion in AnxA6-expressing cells, suggesting that AnxA6-dependent regulation of LE cholesterol distribution impacts cell behavior.

AnxA6, through LE Cholesterol Pathways, Selectively Alters the Location and Function of Stx6—Cholesterol is crucial for membrane biogenesis but also adhesion, trafficking, and signal transduction, all relevant for cell migration and invasion. Certainly, impaired availability of cholesterol through inhibition of

FIGURE 5. *A*, characterization of Stx6 localization in AnxA6-overexpressing cells. CHO-WT and CHO-A6 cells were transfected with Rab11-GFP and stained for Stx6 and VAMP3. *Enlarged areas* show regions of interest. *Arrowheads* indicate co-localization of Stx6 with Rab11 and VAMP3 in CHO-A6 but not CHO-WT cells. Quantification of co-localization between Stx6/Rab11 and Stx6/VAMP3 is shown in the *right panel*. *, $p < 0.05$; **, $p < 0.01$. *B*, same as *A* but in A431-WT and A431-A6 cells. *Scale bars,* 10 μm and 2 μm in panels enlarged areas, respectively. Retrograde transport is not affected in cells expressing elevated AnxA6 levels. Internalization of CTxB in COS-1 (*C*) and STxB in HeLa cells (*D*) transfected with AnxA6-GFP after 5 min, 20 min, and 1 h is shown. The Golgi was labeled with anti-GM130. *Scale bars,* 5 μm. *Insets* show details of the Golgi area in transfected (*1*) and non-transfected (*2*) cells. *Error bars* shown in the figure represent S.D.

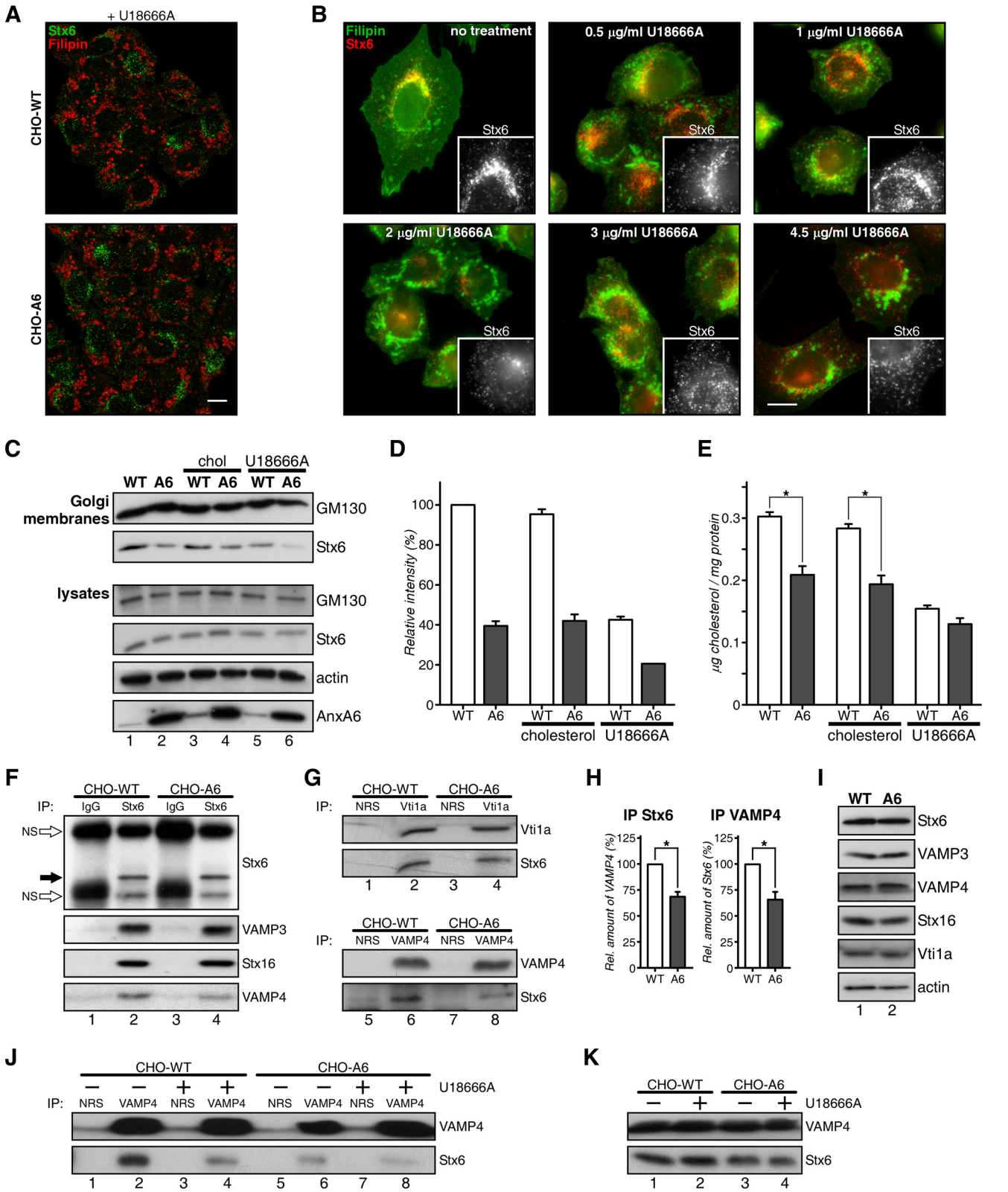

FIGURE 6. **Accumulation of LE cholesterol reduces the association of Stx6 with the TGN.** *A* and *B*, CHO-WT and CHO-A6 cells treated with 3 μg/ml U18666A (*A*) or 0–4.5 μg/ml U18666A for 16 h (*B*) were stained with anti-Stx6 and filipin. *Insets* show Stx6 staining details of the Golgi area. *Scale bars*, 10 μm. *C–E*, Golgi membranes from CHO-WT and CHO-A6 cells ±cholesterol (*chol*) or ±U18666A were isolated. GM130 (Golgi marker), Stx6, and cholesterol (*E*) levels were determined (for Stx6 quantification in Golgi membranes see *D*). GM130, Stx6, actin, and AnxA6 levels in cell lysates are shown. Characterization of Stx6-containing SNARE complexes in CHO-WT and CHO-A6 cells is shown. Stx6 (*F* and *H*), Vti1a (*G*), VAMP4 (*F* and *G*), and control immunoprecipitates were analyzed for co-immunoprecipitation (*IP*) of VAMP3, Stx16, and VAMP4 (*F* and *H*) and Stx6 (*G* and *H*), respectively. Immunoprecipitated Stx6 is shown (*black arrow* in *F*). *H*, quantification of Stx6 and VAMP4 co-precipitations (from *F* and *G*). *I*, Stx6, VAMP3, VAMP4, Stx16, Vti1a, and actin levels in CHO-WT (*WT*) and CHO-A6 (*A6*) in input lysates are comparable. *J*, VAMP4 immunoprecipitates from CHO-WT and CHO-A6 cells ±U18666A were analyzed for Stx6 co-immunoprecipitation. Input lysates are shown in *K*. *NRS*, normal rabbit serum; *NS*, nonspecific (*white arrow*). *, $p < 0.05$. *Error bars* shown in the figure represent S.D.

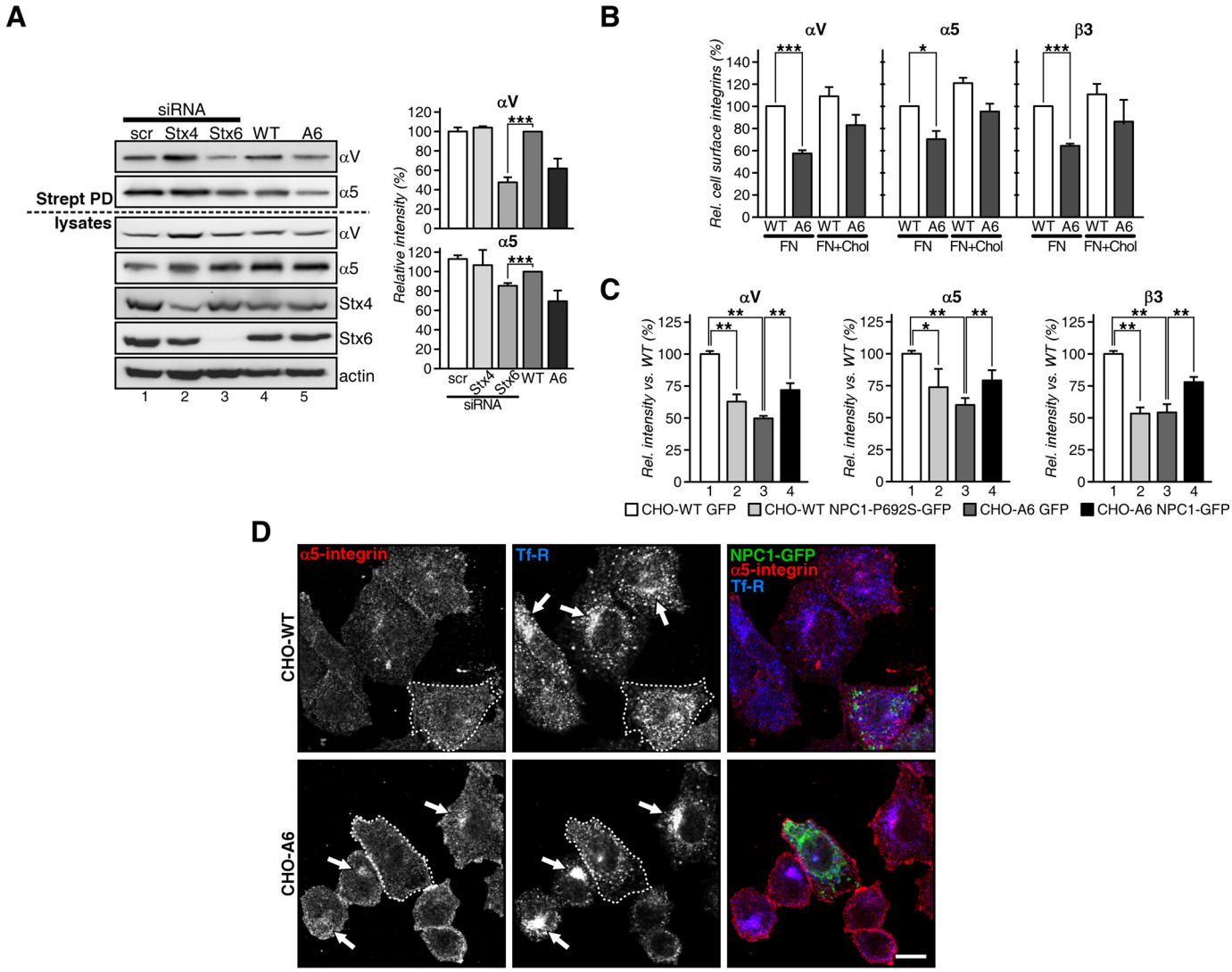

FIGURE 7. *A*, total (*lysates*) and cell surface biotinylated (*Strept PD*) αV and α5 integrins from CHO-WT expressing siRNA targeting Stx4 (*lane 2*) and Stx6 (*lane 3*) and scrambled siRNA (*scr*; *lane 1*) as well as non-transfected CHO-WT (*WT*) and CHO-A6 (*A6*) cells (*lanes 4* and *5*). *B*, exogenous cholesterol restores the recycling of integrins. Cell surface expression of α5, αV, and β3 integrins in CHO-WT and CHO-A6 cells plated on FN and treated ±exogenous cholesterol (30 μg/ml for 90 min). *C*, cell surface expression of α5, αV, and β3 integrins in CHO-WT and CHO-A6 cells expressing control vector (GFP), NPC1-GFP, or NPC1-P692S-GFP was determined by flow cytometry. Values were normalized to CHO-WT. *D*, CHO-WT and CHO-A6 cells were transfected with NPC1-GFP and stained with antibodies for α5 integrin (*red*) and Tf-R (*blue*). *Arrows* indicate perinuclear accumulation of α5 integrin in CHO-A6 (or Tf-R in CHO-WT) cells that is lacking in the NPC1-GFP-transfected cells. *Scale bar*, 10 μm. *, $p < 0.05$; **, $p < 0.01$; ***, $p < 0.001$. *Error bars* shown in the figure represent S.D.

cholesterol synthesis or delivery can affect processes associated with human disease (50).

Vesicular and non-vesicular pathways to export cholesterol from LEs are central for cholesterol trafficking and homeostasis (51, 52). Two annexins, AnxA2 and AnxA6, participate in cholesterol transport through endocytic circuits. In early endosomes, the interplay of AnxA2 with cholesterol regulates biogenesis of multivesicular transport intermediates destined for LEs (53). In LEs, AnxA6 blocks the exit of cholesterol causing an NPC-like phenotype (14, 54). AnxA6 appears to interfere with NPC function because NPC1 overexpression diminished LE cholesterol accumulation and restored trafficking and cellular distribution of caveolin-1 (14) and SNAP23/Stx4 (15).

Here we show that AnxA6, through LE cholesterol pathways, determines TGN association and functioning of Stx6. U18666A treatment or expression of loss-of-function NPC1 mutant in CHO-WT cells also caused disintegration of TGN-associated Stx6. Transient NPC1 expression restored the predominant localization of Stx6 in TGN membranes of CHO-A6 cells. We hypothesize that the reduction of cholesterol in Golgi membranes due to blockage of LE cholesterol egress, observed here and previously (14), together with the reduced formation of Stx6-VAMP4 complexes could explain the retention of Stx6 in the REs. Stx6 knockdown in HeLa cells (55) inhibits retrograde transport, but despite Stx6 mislocalization in CHO-A6 cells, certain pools of Stx6 proteins might still engage normally in multiple other functions in these cells as SNARE complexes with Stx16 and VAMP3 exist and retrograde transport of shiga and cholera toxins to the Golgi was not affected (56). Missorting of Stx6 in REs also did not compromise cation-independent mannose 6-phosphate receptor trafficking in CHO-A6 cells.

However, AnxA6-induced accumulation of Stx6 in the Rab11/VAMP3-positive RE compartment interfered with the recycling of αVβ3 and α5β1 integrins back to the cell surface,

supporting other studies (38, 39). This can be mimicked by depletion of Stx6 but not Stx4, suggesting that AnxA6-mediated changes in cellular cholesterol distribution specifically interfere with some but not all functions of Stx6. In line with these findings, breast cancer MDA-MB-436 cells with high endogenous AnxA6 levels (14) secrete much less TNFα, which requires Stx6 (48), compared with MDA-MB-468 with low levels of endogenous AnxA6 (15).

The underlying mechanisms that enable cholesterol to regulate Stx6 localization in the TGN remain unclear. Cholesterol depletion in the Golgi due to limited LE cholesterol supply likely results in concomitant changes of the lipid environment in TGN microdomains (57). This may interfere with Stx6-VAMP4 complex formation and the interaction of Stx6 with resident Golgi proteins, possibly in specialized cholesterol-rich domains, forcing Stx6 trafficking along secretory pathways to other compartments that provide Stx6 interaction partners.

Stx6-dependent Trafficking of Integrins Is Coordinated by AnxA6 and Cholesterol—AnxA6-mediated cholesterol diminution in Golgi membranes significantly reduced FN secretion (15). Also, in hepatocytes, which contain large amounts of AnxA6 in endosomes (58), the level of ECM proteins (FN and laminin) correlates with the cell surface expression of their cognate integrins or adhesion molecules (59, 60). Actually, we provided the first evidence for the hepatic endocytic compartment modulating the ECM (1). As outlined above, this coincides with Stx6-dependent trafficking of FN receptors αVβ3 and α5β1 integrins (38, 39, 61, 62).

Several studies have associated the localization and function of Stx6 with cholesterol. Similar to the AnxA6-induced changes in caveolin distribution and transport (14), silencing of Stx6 reduced the number of caveolae (42). Furthermore, Stx6 contributes to the functioning of specialized microdomains and focal adhesion sites that contain α5β1 integrin and FAK to participate in the directional migration toward FN (39). Possibly not directly related to Stx6 establishing cholesterol-rich domains at the plasma membrane, Stx6 has been associated with LDL cholesterol transport from LEs to the endoplasmic reticulum via the TGN (63). Our previous study (14) and the data shown here link AnxA6 and inhibition of LE cholesterol egress with Stx6 missorting, which consequently affects cell surface localization and recycling dynamics of the FN receptors αVβ3 and α5β1 integrins.

The role of cholesterol for integrin function is still poorly understood. Cholesterol participates in the formation of signaling complexes containing αVβ3, CD47, and G-proteins (64) and controls cell adhesion and migration onto FN (18). This possibly requires Rab11, which modulates cholesterol transport and homeostasis (65) and facilitates recycling of β1 integrin (37).

Results presented here and previously suggest that the AnxA6-induced cholesterol imbalance impairs integrin recycling in two compartments. (i) Depletion of cholesterol at the plasma membrane increased SNAP23- and Stx4-containing SNARE complexes in the Golgi, consequently reducing their availability as docking/fusion sites at the plasma membrane (15). (ii) Reduced Stx6-VAMP4 complex formation in the TGN caused Stx6 missorting/accumulation in REs.

AnxA6 and Cell Migration—AnxA6 binds to phospholipids, actin, and signaling proteins, which is likely important for cell adhesion and migration. The scaffolding/targeting function of AnxA6 for the GTPase-activating protein p120GAP and protein kinase Cα, both negative regulators of the EGFR/Ras/MAPK pathway, probably contributes to reduce migration/invasion of AnxA6-expressing cells (9, 11, 12, 66). In fact, A431 cells express mutant p53, which drives invasion through constitutive activation of both EGFR and integrin recycling and signaling. Accordingly, inhibiting either EGFR or α5 integrin significantly impeded A431 cell invasion (35). As AnxA6 inhibits EGFR in A431 cells (11, 25) and reduces integrin recycling, the cooperative involvement of both AnxA6 properties could decrease two- and three-dimensional invasion of AnxA6-expressing A431 cells. Data shown here also implicate AnxA6-induced rearrangements of the actin cytoskeleton to contribute to the reduced ability of AnxA6-expressing cells to migrate and invade. AnxA6/actin interactions are mainly based on *in vitro* studies, but we showed that constitutive membrane localization of AnxA6 caused rearrangement and accumulation of F-actin at the plasma membrane (9). Recently, the first evidence from live cells overexpressing AnxA6 supports a model of AnxA6 as an organizer of membrane microdomains and the underlying cytoskeleton (4). Future studies will have to clarify the molecular mechanisms that enable AnxA6 to link cellular cholesterol distribution with actin dynamics in cellular events driving cell migration and invasion.

Author Contributions—C. E., T. G., and C. R. conceived the study and wrote the manuscript. A. G.-M., M. R., E. M.-S., F. M.-P., and A. A.-G. performed the biochemical and immunocytochemical experiments. M. H., M. K., J. R. W. C., C. H. J., Y. A. E., R. Z. M., and P. T. designed and performed the wound healing, two/three-dimensional migration/invasion assays, and integrin experiments. A. P. and F. T. helped in the design and discussion and the molecular biology. All authors reviewed the results and approved the final version of the manuscript.

References

1. Enrich, C., and Evans, W. H. (1987) Evidence for a role of the hepatic endocytic compartment in the modulation of the extracellular matrix. *Exp. Cell Res.* **173,** 99–108
2. Rainero, E., and Norman, J. C. (2013) Late endosomal and lysosomal trafficking during integrin-mediated cell migration and invasion: cell matrix receptors are trafficked through the late endosomal pathway in a way that dictates how cells migrate. *BioEssays* **35,** 523–532
3. De Franceschi, N., Hamidi, H., Alanko, J., Sahgal, P., and Ivaska, J. (2015) Integrin traffic—the update. *J. Cell Sci.* **128,** 839–852
4. Alvarez-Guaita, A., Vilà de Muga, S., Owen, D. M., Williamson, D., Magenau, A., García-Melero, A., Reverter, M., Hoque, M., Cairns, R., Cornely, R., Tebar, F., Grewal, T., Gaus, K., Ayala-Sanmartín, J., Enrich, C., and Rentero, C. (2015) Evidence for annexin A6-dependent plasma membrane remodelling of lipid domains. *Br. J. Pharmacol.* **172,** 1677–1690
5. Gerke, V., Creutz, C. E., and Moss, S. E. (2005) Annexins: linking Ca^{2+} signalling to membrane dynamics. *Nat. Rev. Mol. Cell Biol.* **6,** 449–461
6. Sakwe, A. M., Koumangoye, R., Goodwin, S. J., and Ochieng, J. (2010) Fetuin-A (α_2HS-glycoprotein) is a major serum adhesive protein that mediates growth signaling in breast tumor cells. *J. Biol. Chem.* **285,** 41827–41835
7. Kundranda, M. N., Ray, S., Saria, M., Friedman, D., Matrisian, L. M., Lukyanov, P., and Ochieng, J. (2004) Annexins expressed on the cell surface

serve as receptors for adhesion to immobilized fetuin-A. *Biochim. Biophys. Acta* **1693,** 111–123
8. Takagi, H., Asano, Y., Yamakawa, N., Matsumoto, I., and Kimata, K. (2002) Annexin 6 is a putative cell surface receptor for chondroitin sulfate chains. *J. Cell Sci.* **115,** 3309–3318
9. Monastyrskaya, K., Babiychuk, E. B., Hostettler, A., Wood, P., Grewal, T., and Draeger, A. (2009) Plasma membrane-associated annexin A6 reduces Ca^{2+} entry by stabilizing the cortical actin cytoskeleton. *J. Biol. Chem.* **284,** 17227–17242
10. Sakwe, A. M., Koumangoye, R., Guillory, B., and Ochieng, J. (2011) Annexin A6 contributes to the invasiveness of breast carcinoma cells by influencing the organization and localization of functional focal adhesions. *Exp. Cell Res.* **317,** 823–837
11. Koese, M., Rentero, C., Kota, B. P., Hoque, M., Cairns, R., Wood, P., Vilà de Muga, S., Reverter, M., Alvarez-Guaita, A., Monastyrskaya, K., Hughes, W. E., Swarbrick, A., Tebar, F., Daly, R. J., Enrich, C., and Grewal, T. (2013) Annexin A6 is a scaffold for PKCα to promote EGFR inactivation. *Oncogene* **32,** 2858–2872
12. Vilá de Muga, S., Timpson, P., Cubells, L., Evans, R., Hayes, T. E., Rentero, C., Hegemann, A., Reverter, M., Leschner, J., Pol, A., Tebar, F., Daly, R. J., Enrich, C., and Grewal, T. (2009) Annexin A6 inhibits Ras signalling in breast cancer cells. *Oncogene* **28,** 363–377
13. Koumangoye, R. B., Nangami, G. N., Thompson, P. D., Agboto, V. K., Ochieng, J., and Sakwe, A. M. (2013) Reduced annexin A6 expression promotes the degradation of activated epidermal growth factor receptor and sensitizes invasive breast cancer cells to EGFR-targeted tyrosine kinase inhibitors. *Mol. Cancer* **12,** 167
14. Cubells, L., Vilà de Muga, S., Tebar, F., Wood, P., Evans, R., Ingelmo-Torres, M., Calvo, M., Gaus, K., Pol, A., Grewal, T., and Enrich, C. (2007) Annexin A6-induced alterations in cholesterol transport and caveolin export from the Golgi complex. *Traffic* **8,** 1568–1589
15. Reverter, M., Rentero, C., de Muga, S. V., Alvarez-Guaita, A., Mulay, V., Cairns, R., Wood, P., Monastyrskaya, K., Pol, A., Tebar, F., Blasi, J., Grewal, T., and Enrich, C. (2011) Cholesterol transport from late endosomes to the Golgi regulates t-SNARE trafficking, assembly, and function. *Mol. Biol. Cell* **22,** 4108–4123
16. Navarro-Lérida, I., Sánchez-Perales, S., Calvo, M., Rentero, C., Zheng, Y., Enrich, C., and Del Pozo, M. A. (2012) A palmitoylation switch mechanism regulates Rac1 function and membrane organization. *EMBO J.* **31,** 534–551
17. Freed-Pastor, W. A., Mizuno, H., Zhao, X., Langerød, A., Moon, S. H., Rodriguez-Barrueco, R., Barsotti, A., Chicas, A., Li, W., Polotskaia, A., Bissell, M. J., Osborne, T. F., Tian, B., Lowe, S. W., Silva, J. M., Børresen-Dale, A. L., Levine, A. J., Bargonetti, J., and Prives, C. (2012) Mutant p53 disrupts mammary tissue architecture via the mevalonate pathway. *Cell* **148,** 244–258
18. Ramprasad, O. G., Srinivas, G., Rao, K. S., Joshi, P., Thiery, J. P., Dufour, S., and Pande, G. (2007) Changes in cholesterol levels in the plasma membrane modulate cell signaling and regulate cell adhesion and migration on fibronectin. *Cell Motil. Cytoskeleton* **64,** 199–216
19. Caswell, P. T., Vadrevu, S., and Norman, J. C. (2009) Integrins: masters and slaves of endocytic transport. *Nat. Rev. Mol. Cell Biol.* **10,** 843–853
20. Kanerva, K., Uronen, R. L., Blom, T., Li, S., Bittman, R., Lappalainen, P., Peränen, J., Raposo, G., and Ikonen, E. (2013) LDL cholesterol recycles to the plasma membrane via a Rab8a-Myosin5b-actin-dependent membrane transport route. *Dev. Cell* **27,** 249–262
21. Antalis, C. J., Uchida, A., Buhman, K. K., and Siddiqui, R. A. (2011) Migration of MDA-MB-231 breast cancer cells depends on the availability of exogenous lipids and cholesterol esterification. *Clin. Exp. Metastasis* **28,** 733–741
22. Sun, X., Essalmani, R., Day, R., Khatib, A. M., Seidah, N. G., and Prat, A. (2012) Proprotein convertase subtilisin/kexin type 9 deficiency reduces melanoma metastasis in liver. *Neoplasia* **14,** 1122–1131
23. Danilo, C., and Frank, P. G. (2012) Cholesterol and breast cancer development. *Curr. Opin. Pharmacol.* **12,** 677–682
24. de Diego, I., Schwartz, F., Siegfried, H., Dauterstedt, P., Heeren, J., Beisiegel, U., Enrich, C., and Grewal, T. (2002) Cholesterol modulates the membrane binding and intracellular distribution of annexin 6. *J. Biol. Chem.* **277,** 32187–32194
25. Grewal, T., Heeren, J., Mewawala, D., Schnitgerhans, T., Wendt, D., Salomon, G., Enrich, C., Beisiegel, U., and Jäckle, S. (2000) Annexin VI stimulates endocytosis and is involved in the trafficking of low density lipoprotein to the prelysosomal compartment. *J. Biol. Chem.* **275,** 33806–33813
26. Schneider, C. A., Rasband, W. S., and Eliceiri, K. W. (2012) NIH Image to ImageJ: 25 years of image analysis. *Nat. Methods* **9,** 671–675
27. Cubells, L., Vilà de Muga, S., Tebar, F., Bonventre, J. V., Balsinde, J., Pol, A., Grewal, T., and Enrich, C. (2008) Annexin A6-induced inhibition of cytoplasmic phospholipase A_2 is linked to caveolin-1 export from the Golgi. *J. Biol. Chem.* **283,** 10174–10183
28. Veale, K. J., Offenhäuser, C., Whittaker, S. P., Estrella, R. P., and Murray, R. Z. (2010) Recycling endosome membrane incorporation into the leading edge regulates lamellipodia formation and macrophage migration. *Traffic* **11,** 1370–1379
29. Timpson, P., McGhee, E. J., Morton, J. P., von Kriegsheim, A., Schwarz, J. P., Karim, S. A., Doyle, B., Quinn, J. A., Carragher, N. O., Edward, M., Olson, M. F., Frame, M. C., Brunton, V. G., Sansom, O. J., and Anderson, K. I. (2011) Spatial regulation of RhoA activity during pancreatic cancer cell invasion driven by mutant p53. *Cancer Res.* **71,** 747–757
30. Meijering, E., Dzyubachyk, O., and Smal, I. (2012) Methods for cell and particle tracking. *Methods Enzymol.* **504,** 183–200
31. Dozynkiewicz, M. A., Jamieson, N. B., Macpherson, I., Grindlay, J., van den Berghe, P. V., von Thun, A., Morton, J. P., Gourley, C., Timpson, P., Nixon, C., McKay, C. J., Carter, R., Strachan, D., Anderson, K., Sansom, O. J., Caswell, P. T., and Norman, J. C. (2012) Rab25 and CLIC3 collaborate to promote integrin recycling from late endosomes/lysosomes and drive cancer progression. *Dev. Cell* **22,** 131–145
32. Grewal, T., Evans, R., Rentero, C., Tebar, F., Cubells, L., de Diego, I., Kirchhoff, M. F., Hughes, W. E., Heeren, J., Rye, K. A., Rinninger, F., Daly, R. J., Pol, A., and Enrich, C. (2005) Annexin A6 stimulates the membrane recruitment of p120GAP to modulate Ras and Raf-1 activity. *Oncogene* **24,** 5809–5820
33. Lee, B. Y., Timpson, P., Horvath, L. G., and Daly, R. J. (2015) FAK signaling in human cancer as a target for therapeutics. *Pharmacol. Ther.* **146,** 132–149
34. Timpson, P., Jones, G. E., Frame, M. C., and Brunton, V. G. (2001) Coordination of cell polarization and migration by the Rho family GTPases requires Src tyrosine kinase activity. *Curr. Biol.* **11,** 1836–1846
35. Muller, P. A., Caswell, P. T., Doyle, B., Iwanicki, M. P., Tan, E. H., Karim, S., Lukashchuk, N., Gillespie, D. A., Ludwig, R. L., Gosselin, P., Cromer, A., Brugge, J. S., Sansom, O. J., Norman, J. C., and Vousden, K. H. (2009) Mutant p53 drives invasion by promoting integrin recycling. *Cell* **139,** 1327–1341
36. Caswell, P., and Norman, J. (2008) Endocytic transport of integrins during cell migration and invasion. *Trends Cell Biol.* **18,** 257–263
37. Powelka, A. M., Sun, J., Li, J., Gao, M., Shaw, L. M., Sonnenberg, A., and Hsu, V. W. (2004) Stimulation-dependent recycling of integrin β1 regulated by ARF6 and Rab11. *Traffic* **5,** 20–36
38. Riggs, K. A., Hasan, N., Humphrey, D., Raleigh, C., Nevitt, C., Corbin, D., and Hu, C. (2012) Regulation of integrin endocytic recycling and chemotactic cell migration by syntaxin 6 and VAMP3 interaction. *J. Cell Sci.* **125,** 3827–3839
39. Tiwari, A., Jung, J. J., Inamdar, S. M., Brown, C. O., Goel, A., and Choudhury, A. (2011) Endothelial cell migration on fibronectin is regulated by syntaxin 6-mediated $\alpha5\beta1$ integrin recycling. *J. Biol. Chem.* **286,** 36749–36761
40. Reverter, M., Rentero, C., Garcia-Melero, A., Hoque, M., Vilà de Muga, S., Alvarez-Guaita, A., Conway, J. R., Wood, P., Cairns, R., Lykopoulou, L., Grinberg, D., Vilageliu, L., Bosch, M., Heeren, J., Blasi, J., Timpson, P., Pol, A., Tebar, F., Murray, R. Z., Grewal, T., and Enrich, C. (2014) Cholesterol regulates Syntaxin 6 trafficking at trans-Golgi network endosomal boundaries. *Cell Rep.* **7,** 883–897
41. Bock, J. B., Klumperman, J., Davanger, S., and Scheller, R. H. (1997) Syntaxin 6 functions in trans-Golgi network vesicle trafficking. *Mol. Biol. Cell* **8,** 1261–1271
42. Choudhury, A., Marks, D. L., Proctor, K. M., Gould, G. W., and Pagano, R. E. (2006) Regulation of caveolar endocytosis by syntaxin 6-dependent

delivery of membrane components to the cell surface. *Nat. Cell Biol.* **8,** 317–328
43. Hao, M., Lin, S. X., Karylowski, O. J., Wüstner, D., McGraw, T. E., and Maxfield, F. R. (2002) Vesicular and non-vesicular sterol transport in living cells. The endocytic recycling compartment is a major sterol storage organelle. *J. Biol. Chem.* **277,** 609–617
44. Simonsen, A., Gaullier, J. M., D'Arrigo, A., and Stenmark, H. (1999) The Rab5 effector EEA1 interacts directly with syntaxin-6. *J. Biol. Chem.* **274,** 28857–28860
45. Hsu, V. W., and Prekeris, R. (2010) Transport at the recycling endosome. *Curr. Opin. Cell Biol.* **22,** 528–534
46. Johannes, L., and Popoff, V. (2008) Tracing the retrograde route in protein trafficking. *Cell* **135,** 1175–1187
47. Ikonen, E., and Hölttä-Vuori, M. (2004) Cellular pathology of Niemann-Pick type C disease. *Semin. Cell Dev. Biol.* **15,** 445–454
48. Manderson, A. P., Kay, J. G., Hammond, L. A., Brown, D. L., and Stow, J. L. (2007) Subcompartments of the macrophage recycling endosome direct the differential secretion of IL-6 and TNFα. *J. Cell Biol.* **178,** 57–69
49. Day, P., Riggs, K. A., Hasan, N., Corbin, D., Humphrey, D., and Hu, C. (2011) Syntaxins 3 and 4 mediate vesicular trafficking of alpha5beta1 and alpha3beta1 integrins and cancer cell migration. *Int. J. Oncol.* **39,** 863–871
50. Maxfield, F. R., and van Meer, G. (2010) Cholesterol, the central lipid of mammalian cells. *Curr. Opin. Cell Biol.* **22,** 422–429
51. Ikonen, E. (2008) Cellular cholesterol trafficking and compartmentalization. *Nat. Rev. Mol. Cell Biol.* **9,** 125–138
52. Du, X., Kumar, J., Ferguson, C., Schulz, T. A., Ong, Y. S., Hong, W., Prinz, W. A., Parton, R. G., Brown, A. J., and Yang, H. (2011) A role for oxysterol-binding protein-related protein 5 in endosomal cholesterol trafficking. *J. Cell Biol.* **192,** 121–135
53. Mayran, N., Parton, R. G., and Gruenberg, J. (2003) Annexin II regulates multivesicular endosome biogenesis in the degradation pathway of animal cells. *EMBO J.* **22,** 3242–3253
54. Domon, M., Nasir, M. N., Matar, G., Pikula, S., Besson, F., and Bandorowicz-Pikula, J. (2012) Annexins as organizers of cholesterol- and sphingomyelin-enriched membrane microdomains in Niemann-Pick type C disease. *Cell. Mol. Life Sci.* **69,** 1773–1785
55. Ganley, I. G., Espinosa, E., and Pfeffer, S. R. (2008) A syntaxin 10-SNARE complex distinguishes two distinct transport routes from endosomes to the trans-Golgi in human cells. *J. Cell Biol.* **180,** 159–172
56. Mallard, F., Tang, B. L., Galli, T., Tenza, D., Saint-Pol, A., Yue, X., Antony, C., Hong, W., Goud, B., and Johannes, L. (2002) Early/recycling endosomes-to-TGN transport involves two SNARE complexes and a Rab6 isoform. *J. Cell Biol.* **156,** 653–664
57. Duran, J. M., Campelo, F., van Galen, J., Sachsenheimer, T., Sot, J., Egorov, M. V., Rentero, C., Enrich, C., Polishchuk, R. S., Goñi, F. M., Brügger, B., Wieland, F., and Malhotra, V. (2012) Sphingomyelin organization is required for vesicle biogenesis at the Golgi complex. *EMBO J.* **31,** 4535–4546
58. Jäckle, S., Beisiegel, U., Rinninger, F., Buck, F., Grigoleit, A., Block, A., Gröger, I., Greten, H., and Windler, E. (1994) Annexin VI, a marker protein of hepatocytic endosomes. *J. Biol. Chem.* **269,** 1026–1032
59. Stamatoglou, S. C., Enrich, C., Manson, M. M., and Hughes, R. C. (1992) Temporal changes in the expression and distribution of adhesion molecules during liver development and regeneration. *J. Cell Biol.* **116,** 1507–1515
60. Pujades, C., Forsberg, E., Enrich, C., and Johansson, S. (1992) Changes in cell surface expression of fibronectin and fibronectin receptor during liver regeneration. *J. Cell Sci.* **102,** 815–820
61. Skalski, M., and Coppolino, M. G. (2005) SNARE-mediated trafficking of $\alpha5\beta1$ integrin is required for spreading in CHO cells. *Biochem. Biophys. Res. Commun.* **335,** 1199–1210
62. Timpson, P., McGhee, E. J., Erami, Z., Nobis, M., Quinn, J. A., Edward, M., and Anderson, K. I. (2011) Organotypic collagen I assay: a malleable platform to assess cell behaviour in a 3-dimensional context. *J. Vis. Exp.* **56,** e3089
63. Urano, Y., Watanabe, H., Murphy, S. R., Shibuya, Y., Geng, Y., Peden, A. A., Chang, C. C., and Chang, T. Y. (2008) Transport of LDL-derived cholesterol from the NPC1 compartment to the ER involves the trans-Golgi network and the SNARE protein complex. *Proc. Natl. Acad. Sci. U.S.A.* **105,** 16513–16518
64. Green, J. M., Zhelesnyak, A., Chung, J., Lindberg, F. P., Sarfati, M., Frazier, W. A., and Brown, E. J. (1999) Role of cholesterol in formation and function of a signaling complex involving $\alpha v\beta3$, integrin-associated protein (CD47), and heterotrimeric G proteins. *J. Cell Biol.* **146,** 673–682
65. Hölttä-Vuori, M., Tanhuanpää, K., Möbius, W., Somerharju, P., and Ikonen, E. (2002) Modulation of cellular cholesterol transport and homeostasis by Rab11. *Mol. Biol. Cell* **13,** 3107–3122
66. Grewal, T., and Enrich, C. (2006) Molecular mechanisms involved in Ras inactivation: the annexin A6-p120GAP complex. *BioEssays* **28,** 1211–1220